ACCSCIENCE PUBLISHING

International Journal of Bioprinting

RESEARCH ARTICLE

Spatially defined bioprinting of detrusor and sphincter mimetics uncovers paracrine-mediated contraction dyssynergia

Weilun Zhang[1], Yuxin Zhang[1], Chengzhi Zhang[1], Haowei Song[1], Yuexian Liu[1], Yutong Li[1], Yipeng Zhao[1], Zhen Zhang[1], Wenbo Zhai[1], Yi Rong[2], Jingtang Hu[2], Weibing Shuang[2], Xueling Yan[1], Junya Shi[1], Xiaodong Wen[1], and Lei Pang[1]*

[1]Department of Urology, Fifth Hospital of Shanxi Medical University (Shanxi Provincial People's Hospital), Taiyuan, Shanxi, China

[2]Department of Urology, First Hospital of Shanxi Medical University, Taiyuan, Shanxi, China

Abstract

Detrusor-sphincter dyssynergia (DSD) represents a core functional impairment of the neurogenic bladder following spinal cord injury; however, no model exists that recapitulates the three-dimensional tissue architecture of the detrusor-sphincter unit and enables analysis of cell–cell communication *in vitro*. In this study, an innovative spatially defined bioprinting strategy was developed to construct parallel-aligned tissue structures of detrusor smooth muscle cells and urethral sphincter fibroblasts. By precisely controlling the inter-tissue distance to 200 μm, a microenvironment that permits paracrine signaling but prevents direct cell–cell contact was developed. Upon stimulation with inflammatory factors mimicking the pathological state after spinal cord injury, this model enabled, for the first time, visualization and quantitative analysis of the transition of detrusor contractions from synchronous to asynchronous and out-of-phase under the regulation of sphincter-derived paracrine signals. Mechanistic investigations revealed that sphincter fibroblasts specifically upregulate and secrete connective tissue growth factor (CTGF) under pathological conditions, which induces aberrant detrusor contractions via the integrin αvβ3/focal adhesion kinase/extracellular signal-regulated kinase signaling pathway. Neutralizing antibodies against CTGF or the clinical drug mirabegron significantly restored contractile coordination. This study not only provides the first quantifiable *in vitro* dual-tissue model for DSD research but also uncovers a local inter-tissue communication disorder mechanism independent of neural innervation, opening new avenues for targeted therapy of neurogenic bladder.

Keywords: Three-dimensional bioprinting; Detrusor-sphincter dyssynergia; Paracrine signaling; Tissue engineering; Cell–cell communication; Connective tissue growth factor

***Corresponding author:**
Lei Pang
(pauldoctor@sxmu.edu.cn)

Citation: Zhang W, Zhang Y, Zhang C, *et al*. Spatially defined bioprinting of detrusor and sphincter mimetics uncovers paracrine-mediated contraction dyssynergia. *Int J Bioprint.* 2026;12(4):026240252. doi: 10.36922/IJB026240252

Received: June 11, 2026

Revised: July 7, 2026

Accepted: July 13, 2026

Published online: July 13, 2026

1. Introduction

Detrusor-sphincter dyssynergia (DSD) is a clinically important manifestation of spinal cord injury (SCI)-induced lower urinary tract dysfunction, characterized by impaired

coordination between detrusor contraction and urethral sphincter relaxation and commonly evaluated using urodynamic and electromyographic methods.[1-3] SCI can also induce structural and molecular remodeling of the bladder wall, including fibrosis.[4] This discoordination during voiding can lead to high intravesical pressure, reflux, upper urinary tract deterioration, and renal impairment.[5] While DSD research has traditionally centered on central neural circuit imbalances,[5,6] emerging evidence implicates local microenvironmental changes in the bladder and urethra after SCI,[7] suggesting that disordered inter-tissue paracrine communication may constitute an overlooked pathogenic mechanism.[8,9]

Three-dimensional (3D) bioprinting enables the fabrication of multicellular, multi-tissue constructs with precise spatial organization.[10,11] However, most studies have focused on single tissues and have not exploited the spatial precision of bioprinting to probe inter-tissue functional interactions.[11] We hypothesized that the post-SCI pathological microenvironment disrupts paracrine signaling between detrusor and sphincter cells, thereby inducing contractile incoordination, and that bioprinting offers an ideal tool for the investigation. Specifically, we leveraged the following advantages: (i) Spatial precision—independent control of inter-tissue distance, permitting paracrine communication while eliminating direct cell–cell contact;[12,13] (ii) microenvironment preservation—tunable bioinks (e.g., gelatin methacryloyl [GelMA]) that maintain cell phenotypes and tissue mechanical properties;[12] (iii) functional readout—printed strips exhibit spontaneous rhythmic contractions, enabling image-based quantification of contraction coordination;[13] and (iv) mechanistic intervenability—pharmacological and antibody-based perturbations can be directly applied to dissect signaling axes.[12,13] These features allow the bioprinted model to isolate the effect of distance-dependent paracrine signaling on contraction coordination. We defined *in vitro* contraction dyscoordination as loss of phase synchrony between the two tissues and quantified it using a newly developed contraction coordination index (CCI). Based on this, we established a spatially defined bioprinting strategy to generate parallel-aligned strips of rat detrusor and sphincter cells separated by 200 μm, a distance that permits paracrine communication.[11,14] Under SCI-mimicking inflammatory conditions, we achieved the first visualization and quantitative assessment of contraction dyscoordination,[15] and further dissected the molecular mechanisms driving this process.

2. Materials and methods

2.1. Cell culture

Rat primary bladder smooth muscle cells (PXRS-C196, HyCyte, China) were purchased and cultured in the recommended complete medium (PXRS-C196, HyCyte, China). Rat urethral sphincter fibroblasts were isolated and identified from the urethral sphincter tissue of Sprague–Dawley rats (n = 5) in our laboratory and cultured in fibroblast-specific medium. All cells were maintained in a cell culture incubator. For passaging, cells were detached using 0.25% trypsin, 0.04% ethylenediaminetetraacetic acid, and passages three to five were used for subsequent experiments.

2.2. Bioink preparation and three-dimensional bioprinting

Gelatin methacryloyl (synthesized in our laboratory) was used as the bioink, dissolved in sterile phosphate-buffered saline, and supplemented with 0.25% photoinitiator (lithium phenyl[2,4,6-trimethylbenzoyl]phosphinate). Rat primary bladder smooth muscle cells or urethral sphincter fibroblasts were gently mixed with the GelMA solution at a density of 1×10^5 cells/mL. Parallel strips were printed under sterile conditions using a modified desktop extrusion-based bioprinter (EFL-BP8601 Ultra, Suzhou Yongqinquan Intelligent Equipment Co., Ltd., China) equipped with a conical needle of 250 μm inner diameter. Immediately after printing, the constructs were crosslinked using 405 nm ultraviolet (UV) light,[16] followed by the addition of culture medium and incubation in a cell culture incubator. For the dual-tissue model, detrusor strips and sphincter strips were arranged in parallel with a precisely controlled inter-strip distance of 200 μm.[17]

To maintain a constant inter-strip distance of 200 μm throughout the culture period, several precautions were taken. While the designed value was 200 μm, the actual spacing of the low-concentration GelMA (5%) after swelling was 196 ± 8 μm, which is acceptable for the study. To ensure the spatial fidelity in the printing, the following measures were taken: (i) Two-step crosslinking: Low-temperature physical crosslinking (4 °C, 10 min) and UV photocrosslinking (405 nm, 30 s) were combined to guarantee printing accuracy and dimensional stability; (ii) swelling pre-equilibration: All printed constructs were allowed to swell in culture medium for 12 h prior to the formal experiments to equilibrate the hydrogel before measurements were taken. The design spacing was determined to be 185 μm, after swelling to the target spacing of 200 μm based on the swelling coefficient obtained in the pre-experiments. (c) Osmotic control: throughout, media were used without phenol red, and the osmotic pressure was kept at 280–320 mOsm/L to minimize the effects of osmotic fluctuation on the swelling behavior.[18] Inter-strip spacing was observed on days 1, 3, 5, and 7 of the seven-day culture period. Following pre-equilibration, the spacing was stable, and no significant drift ($p > 0.05$) was noted.

2.3. Simulation of pathological microenvironment

To simulate the inflammatory microenvironment following SCI, the basal culture medium was supplemented with recombinant rat tumor necrosis factor (TNF)-α (10 ng/mL; Cat# 400-14, PeproTech, United States of America [USA]), nerve growth factor (NGF) (50 ng/mL; Cat# 556-NG, R&D Systems, USA), and ATP (100 μM; Cat# A7699, Sigma-Aldrich, USA), and cells were cultured under pathological stimulation for 24–48 hours. These concentrations were selected based on dose-response pilot experiments and were consistent with concentrations employed in established *in vitro* SCI-mimetic models.[19] The concentrations selected are in the pathophysiological range found in human SCI patients, where levels of TNF-α are greatly elevated in both serum (50–200 pg/mL) and cerebrospinal fluid, NGF is upregulated in the bladder wall and urine, and extracellular ATP is released from damaged cells and activated inflammatory cells at the injury site in the micromolar range.[20,21] The *in vitro* stimulation regimen therefore mimics important features of the tonic inflammatory environment, thereby supporting local tissue modification in the neurogenic bladder.

2.4. Analysis of contractile function and calculation of coordination index

To obtain a time-lapse series of images of the printed tissue strips, an inverted microscope (4× objective; Ti-E, Nikon, Japan) with an incubating stage (37 °C, 5% carbon dioxide) was used. Under these conditions, time-lapse images were taken every 15 s for 45 min (180 frames). The computational workflow comprised the following steps:

- Particle image velocimetry (PIV) analysis of time-series images: The images were imported into OpenPIV, an open-source PIV toolbox, and the displacement field was calculated frame-by-frame for each region of interest (ROI) using a fast Fourier transform-based cross-correlation algorithm with a 64 × 64-pixel interrogation window and a 50% overlap.
- Time-series image: The images were imported into OpenPIV, and the displacement field was calculated frame-by-frame for each ROI using a fast Fourier transform-based cross-correlation algorithm with a 64 × 64-pixel interrogation window and a 50% overlap.[22]
- Centroid trajectory extraction: After ROI-segmenting each strip region separately (detrusor and sphincter), spatial integration of the displacement field data was performed to obtain the coordinates of the centroid xd(t) and xs(t) at every time point, resulting in two separate displacement-time curves for detrusor and sphincter.
- CCI calculation: The normalized cross-correlation function of the two curves was calculated, and the maximum value of the cross-correlation function was the CCI. CCI values range from 0 to 1, with values close to 1 indicating highly synchronous contraction phases and those close to 0 indicating desynchronization or anti-phase contraction phases. All computational analysis was performed using custom MATLAB scripts (R2021a, MathWorks, USA) developed in-house and integrated with the OpenPIV toolbox, as previously described.[23,24]

The CCI values reported in this study (0.80 ± 0.04 for normal, 0.26 ± 0.07 for pathological conditions) represent the mean ± standard deviation (SD) across three independent biological replicates (n = 3), each consisting of a separate bioprinting experiment and image acquisition session. Based on the distribution of CCI values in the normal control group, we propose a tentative threshold for normal synchronous contraction at CCI ≥ 0.70, corresponding to the lower bound of the 95% confidence interval (mean − 2SD) of the normal group. CCI values between 0.50 and 0.70 may indicate moderate dyscoordination, while CCI < 0.50 indicates severe contraction dyssynergia. This approach is consistent with quantitative synchronization analyses in other excitable tissues, including cardiomyocyte sheets (where cross-correlation analysis is routinely used to assess contraction synchrony) and gastrointestinal smooth muscle. While these thresholds are model-specific and require clinical validation, they provide a quantitative framework for classifying contraction phenotypes in future DSD studies.

2.5. Collection of conditioned medium and assessment of paracrine efficiency

Conditioned media were collected from the dual-tissue models with different inter-strip distances (100, 200, and 500 μm) and centrifuged to remove cell debris. The resulting conditioned media were then transferred to freshly printed detrusor strips and cultured for 24 h. Cell proliferation activity was assessed using the cell counting kit-8 (CCK-8; CK04, Dojindo Laboratories, Japan) assay. Diffusion efficiency of paracrine factors was evaluated using a fluorescent dextran (fluorescein isothiocyanate-dextran, 10 kDa) diffusion assay:[18] the fluorescent dye was added to one side of the sphincter strip, and the fluorescence intensity was measured on the detrusor strip side at different time points.

2.6. Cytokine array and enzyme-linked immunosorbent assay

The cytokine secretion profiles of sphincter fibroblasts under normal or pathological conditions were detected using a rat cytokine antibody array. The procedure was performed according to the manufacturer's instructions,

and semi-quantitative analysis was performed using chemiluminescence imaging and grayscale value measurements. Connective tissue growth factor (CTGF) secretion levels were determined using an enzyme-linked immunosorbent assay (ELISA) kit (ab275897, Abcam, United Kingdom [UK]) to measure CTGF concentration in the conditioned medium. Experiments were repeated three times.

2.7. Quantitative real-time polymerase chain reaction

Total RNA was extracted from cells using TRIzol and reverse-transcribed into cDNA. Amplification was performed using SYBR Green Master Mix (Bio-Rad, USA) on a CFX96 real-time polymerase chain reaction (PCR) system (Bio-Rad, USA). The primer sequences for rat *Ccn2*, which encodes CTGF, were obtained from a previous study:[25] forward, 5'-GGCCTGTGAAGCTGACCTAG-3'; reverse, 5'-GCCCGGTAGGTCTTCACACTG-3'. *Gapdh* was used as an internal control. Relative expression levels were calculated using the $2^{-\Delta\Delta Ct}$ method.

2.8. Western blot

Proteins were lysed using radioimmunoprecipitation assay lysis buffer, and protein concentrations were determined using the bicinchoninic acid method. Protein samples (30 μg) were separated using sodium dodecyl sulfate-polyacrylamide gel electrophoresis and transferred onto polyvinylidene fluoride membranes. After blocking with non-fat milk, the membranes were incubated with primary antibodies against integrin αvβ3 (ab78269, Abcam, UK), low-density lipoprotein receptor-related protein 1 (LRP1) (ab92544, Abcam, UK), p-focal adhesion kinase (FAK) (Tyr397; 3283, Cell Signaling Technology, USA), total FAK (3285, Cell Signaling Technology, USA), p-extracellular signal-regulated kinase (ERK) 1/2 (Thr202/Tyr204; 4370, Cell Signaling Technology, USA), total ERK (4695, Cell Signaling Technology, USA), and GAPDH (5174, Cell Signaling Technology, USA). After overnight incubation at 4 °C, the membranes were incubated with horseradish peroxidase-conjugated secondary antibodies at room temperature, and signals were visualized using enhanced chemiluminescence. Grayscale values were quantified using ImageJ software (Version 1.53r, National Institutes of Health, USA).

2.9. Inhibitor and neutralizing antibody intervention experiments

The following inhibitors were added one hour prior to pathological stimulation: the integrin αvβ3 inhibitor cilengitide,[19] a FAK inhibitor, and the ERK pathway inhibitor U0126. CTGF-neutralizing antibody was added to the culture medium simultaneously with pathological stimulation. Mirabegron was added at concentrations ranging from 1 to 20 μM. After intervention, cells were cultured for an additional 24 h, followed by contraction analysis or protein detection.

2.10. Small interfering RNA knockdown experiments

Small interfering RNA (siRNA) targeting the rat integrin β3 subunit (SASI_Rn01_00012345, Sigma-Aldrich, USA) was used to transfect detrusor smooth muscle cells using Lipofectamine RNAiMAX (Invitrogen, USA). Forty-eight hours after transfection, knockdown efficiency (> 70%) was verified via western blotting. The knockdown cells were then used for bioprinting and subsequent CTGF stimulation experiments. A scrambled negative control siRNA was used as the control for nonspecific effects.

2.11. Immunofluorescence staining

Immunofluorescence staining was performed to assess the expression and subcellular localization of integrin αvβ3 in detrusor smooth muscle cells within the bioprinted constructs. Printed constructs were fixed with 4% paraformaldehyde for 30 min at room temperature, permeabilized with 0.25% Triton X-100 for 15 min, and blocked with 5% bovine serum albumin in phosphate-buffered saline (PBS) for 1 h at room temperature. The samples were then incubated overnight at 4°C with primary antibody against integrin αvβ3 (working dilution 1:200; ab78269, Abcam, UK). After three washes with PBS, the constructs were incubated with goat anti-mouse IgG Alexa Fluor 488-conjugated secondary antibody (working dilution 1:1,000; ab150117, Abcam, UK) for 1 h at room temperature in the dark. Nuclei were counterstained with 4',6-diamidino-2-phenylindole (DAPI; 1 μg/mL; Sigma-Aldrich, USA) for 5 min. Fluorescence images were acquired using a confocal laser scanning microscope. Membrane fluorescence intensity was quantified using ImageJ software (Version 1.53), and at least three randomly selected fields per sample were analyzed for each experimental condition. All experiments were repeated three times independently.

2.12. Statistical analysis

All experiments were independently repeated at least three times, and data are presented as mean ± SD unless otherwise stated. Statistical analysis was performed using GraphPad Prism (version 9.0, GraphPad Software, Inc., USA). For comparisons between two groups (e.g., normal vs. pathological CCI, control vs. treatment groups), an unpaired two-tailed Student's *t*-test was used. For comparisons among three or more groups (e.g., dose-response experiments, multiple inhibitor treatments,

different inter-strip distance groups), one-way analysis of variance (ANOVA) followed by Tukey's post-hoc multiple comparison test was employed. For time-course experiments, a two-way ANOVA with Bonferroni post hoc correction was applied. The normality of the data distribution was verified using the Shapiro–Wilk test, and the homogeneity of variances was assessed using Levene's test. For CCI analysis, video data were assigned coded identifiers by an independent investigator, and the MATLAB-based analysis was performed by a separate researcher blinded to group allocation. Blinding was maintained until all quantitative parameters were extracted. Significance levels were set at $^{*}p < 0.05$, $^{**}p < 0.01$, and $^{***}p < 0.001$. Exact p-values are reported in figure legends and in the text for key comparisons.

3. Results

3.1 Construction and optimization of the spatially defined dual-tissue model

In this study, a spatially defined 3D bioprinted dual-tissue model was constructed to simulate paracrine communication and contractile coordination between the detrusor and the urethral sphincter *in vitro*. The study design and model fabrication scheme are shown in Figure 1A. We first performed rheological screening of three bioinks: collagen I, GelMA, and alginate. The results indicated that GelMA exhibited the best shear-thinning property within a shear rate range of 0.1–200 s^{-1}, making it suitable for extrusion-based bioprinting (Figure 1B). Dynamic frequency-sweep measurements showed that the storage modulus (G') of GelMA remained higher than the loss modulus (G"), indicating a stable, solid-like mechanical behavior that maintains structural integrity after printing (Figure 1C). Cell viability results showed that a cell density of 1×10^5 cells/mL was optimal. At this density, the cells maintained high viability at 24 h, 72 h, and 7 days post-printing, with values of 89.7 ± 2.1%, 86.5 ± 2.8%, and 83.2 ± 3.1%, respectively; higher cell densities led to decreased viability (Figure 1D). The dual-strip-printed constructs exhibited well-defined boundaries and morphology under the optimized parameters. The width of detrusor smooth muscle strips was 1.85 ± 0.12 mm, with a thickness of 0.82 ± 0.07 mm, and the width of sphincter fibroblast strips was 1.78 ± 0.01 mm, and the thickness was 0.79 ± 0.06 mm, showing good structural stability and reproducibility (Figure 1E). Using the bioink and rat primary bladder smooth muscle cells, a 3D model of a long porous scaffold (Figure 1F) was fabricated using a digital light processing (DLP) based 3D printer, with the detrusor strips as the printed product. Figure 1Gi shows the morphology of a single strip immediately after printing, and Figure 1Gii shows its microscopic image. The strips were cultured in a specific medium and survived for three days, with observations made every other day. Figures 1Giii and 1Giv are the microscopic images taken on day one of culture under low and high magnification, respectively. Figures 1Gv and 1Gvi are the images taken on day three, with each panel including both high-magnification and low-magnification views.[26]

3.2. Regulation of paracrine communication by tissue spacing

In the constructed dual-tissue bioprinted model, we further investigated the regulatory effect of inter-tissue distance on paracrine communication efficiency (Figure 2). We designed and printed dual-strip constructs with three different inter-strip distances: 100, 200, and 500 μm. Microscopic observation showed that the actual printed dimensions were consistent with the design values, and the morphology, width, and thickness of the strips remained stable across groups (Figure 2A). Fluorescent dye diffusion experiments were used to quantitatively assess the transfer efficiency of paracrine factors, confirming that a 200 μm distance enabled effective diffusion while preventing direct cell contact or transmigration (Figure 2B). To validate the effect of distance-dependent paracrine signaling on cellular function, we collected conditioned media from the different distance groups and applied them to detrusor smooth muscle cells (Figure 2C). According to the schematic diagram, at the paracrine factor, the cell proliferation activity at different paracrine factor origin distances is significantly different, and the paracrine factor origin distance of 200 μm showed the strongest paracrine effect (Figure 2D). In addition, cytokine array and transcriptomic analyses showed that several key cytokines and intercellular communication molecules were significantly induced in the 200 μm distance group compared to the control group, indicating that this distance is optimal for paracrine crosstalk (Figure 2E). This study, using paracrine efficiency, determined that the optimal inter-tissue distance is 200 μm, but this has yet to be confirmed for the coordination of contractions.

3.3. The pathological microenvironment induces contraction dyssynergia

Based on the established spatially defined dual-tissue model, we further simulated the pathological microenvironment following SCI and systematically investigated the effects of inflammatory cytokine stimulation on contraction coordination between the detrusor and the sphincter fibroblast-derived component, followed by multi-dimensional quantitative analysis of their dynamic phenotypes (Figure 3). From the representative time-series images in Figure 3A, the control group exhibited rhythmic

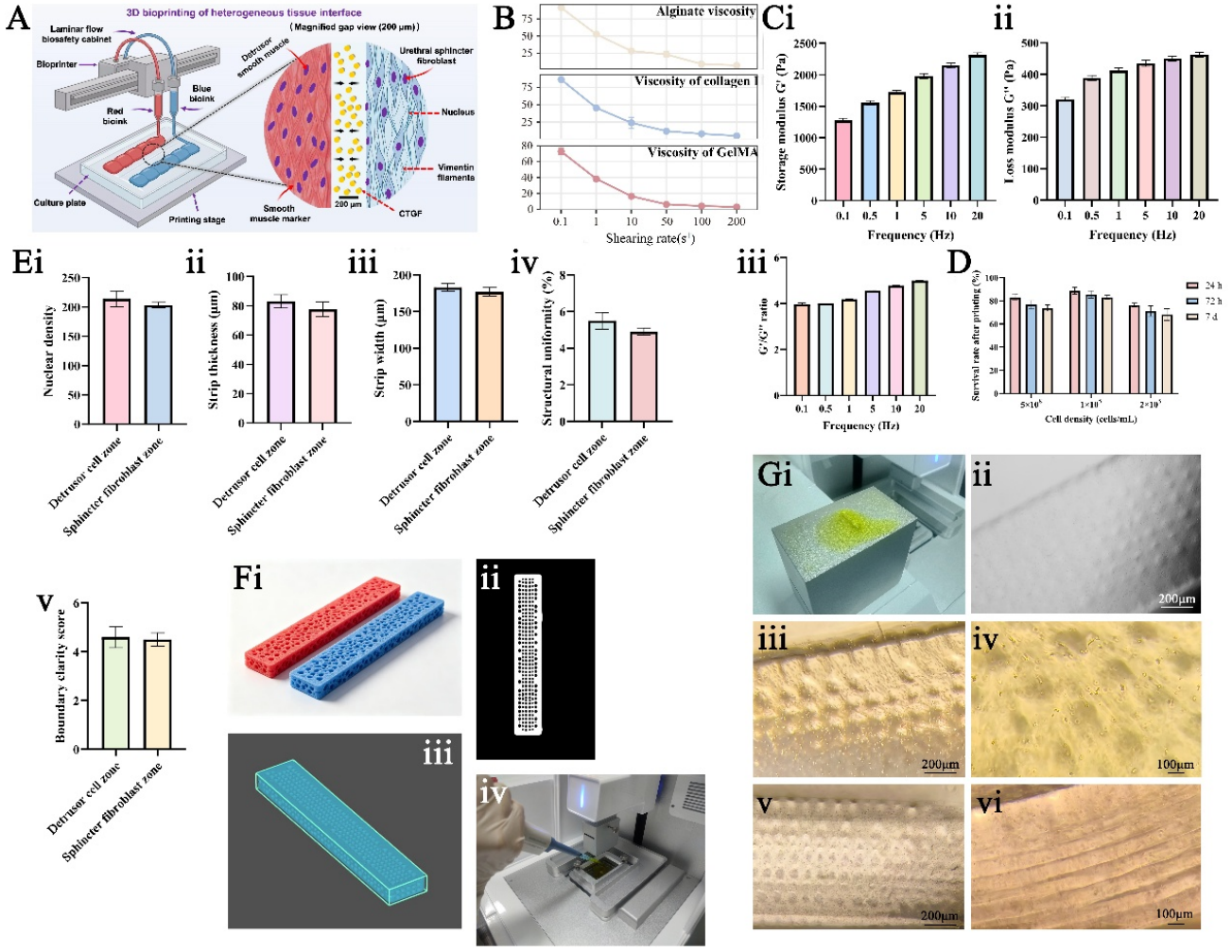

Figure 1. Construction and optimization of the spatially defined dual-tissue model. (A) Schematic diagram of the study design, illustrating the use of three-dimensional (3D) bioprinting to construct a paracrine-dependent inter-tissue communication model with spatially precise separation between detrusor smooth muscle cells and urethral sphincter fibroblasts. (B) Rheological characterization of three bioinks (collagen I, gelatin methacryloyl [GelMA], and alginate) under physiological shear rates (0.1–200 s^{-1}). GelMA exhibited shear-thinning behavior, making it well-suited for extrusion-based printing. (C) Frequency-dependent viscoelastic plot of GelMA. The storage modulus (G') remained higher than the loss modulus (G") across the tested frequencies, indicating stable solid-like mechanical behavior that maintains structural integrity after printing. (D) Cell viability of printed constructs at three seeding densities, measured at 24 h, 72 h, and seven days. The group with a density of 1×10^5 cells/mL showed the highest long-term viability. (E) Morphological quantification of the optimized dual-strip constructs. The printed detrusor strips and sphincter strips exhibited uniform morphology, clear boundaries, and stable dimensions. (F) Multi-angle 3D images of a long porous scaffold (Panels i–iii), which provides physical support for cell attachment and tissue growth. Panel iv shows extrusion-based bioprinting of a biological strip, leveraging the high precision of a digital light processing (DLP)-based 3D printer. (G) Viability and morphology observation of 3D-bioprinted detrusor strips on the scaffold. Panel i shows a photograph of a single strip within 10 min after printing. Panel ii shows a microscopic image of the strip within 30 min after printing. Scale bar: 200 μm; magnification: 4×. (Panels iii) and iv show the strip on day one after printing. Scale bars: 200 μm, 100 μm; magnifications: 4×, 10×. (Panels v) and (vi) show the strip on day three after printing. Scale bars: 200 μm, 100 μm; magnifications: 4×, 10×. Images in all panels are representative of three independent experiments.

synchronous contractions, whereas the pathological group showed marked asynchronous contractions. Dynamic motion amplitude analysis (Figure 3B) revealed significantly increased tissue dispersion and markedly decreased contraction regularity under pathological conditions. Quantitative comparison of the time series of centroid displacement (Figure 3C) indicated a clear phase shift between the detrusor and sphincter tissues in the pathological group. Statistical analysis of the CCI (Figure 3D) showed that the value decreased significantly from 0.8 ± 0.04 in the control group to 0.26 ± 0.07 in the pathological group (***$p < 0.001$). In addition, power

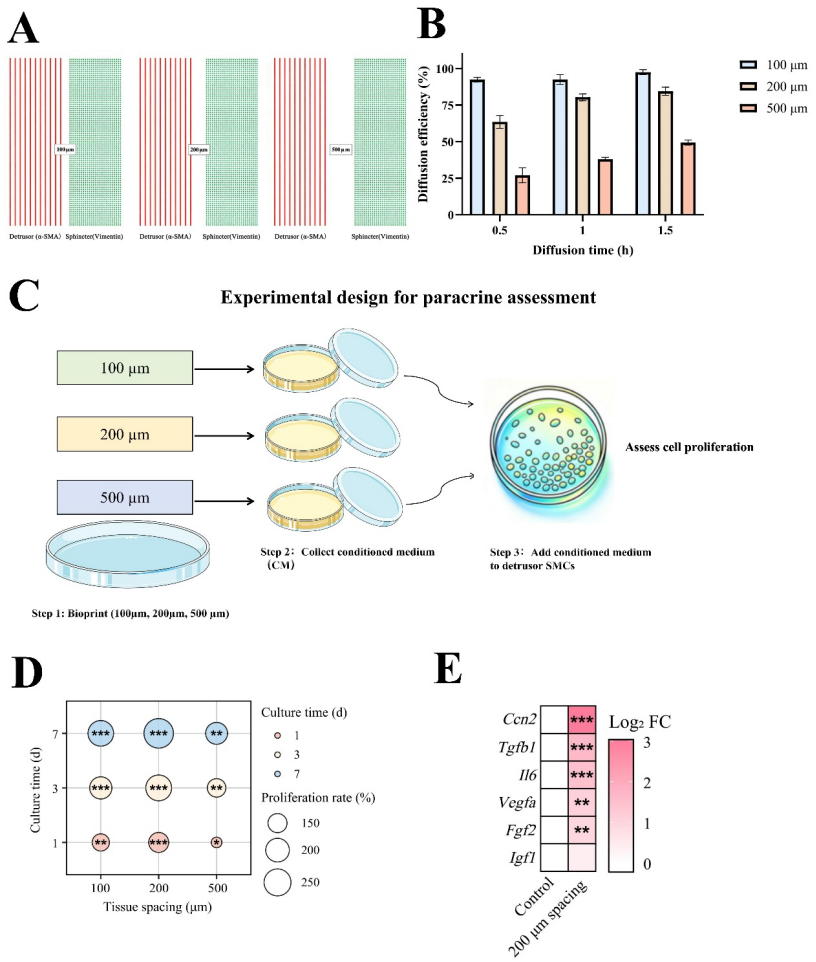

Figure 2. Regulation of paracrine communication by tissue spacing in the bioprinted dual-tissue model. (A) Schematic of printed dual-tissue structures with varying inter-tissue spacing (100, 200, and 500 μm). Printed dimensions closely matched the design, and the width and thickness of the strip were uniform within each spacing group. (B) Measurement of diffusion efficiency of the paracrine factors of different tissue spacings by a fluorescent dye transfer assay. Results show that molecular exchange is effective at a spacing of 200 μm, while direct cell contact is prevented. (C) Schematic of conditioned medium (CM) exchange experiment for the evaluation of paracrine signaling. CM from the various spacings was harvested and added to the recipient culture for assessment of its effect. (D) Effect of paracrine factors under the different spacing conditions on the proliferation rate of detrusor smooth muscle cells. Spacing-dependent CM significantly modulated proliferation, with the 200 μm group showing the greatest effect. (E) Heatmap of gene expression profiles associated with paracrine under 200 μm spacing compared to control. Important signaling molecules involved in inter-tissue communication are significantly upregulated in transcriptomic analysis. Notes: $^{*}p < 0.05$; $^{**}p < 0.01$; $^{***}p < 0.001$.

spectral density analysis (Figure 3E) revealed a disturbance of the contraction rhythm in the pathological group, with the dominant frequency significantly increased. Figure 3A–3E, taken together, illustrate the severe impairment of the coordinated contraction ability of the detrusor/bladder neck unit of the pathological microenvironment.

Cell viability under pathological stimulation was monitored to exclude the possibility that the observed contraction dyssynergia resulted from cytotoxicity. CCK-8 assay of the dual-tissue constructs at 24 h, 72 h, and 7 days under pathological conditions revealed cell viability consistently exceeding 80% at all time points, comparable to the viability observed under normal culture conditions (data shown in Figure 1D for normal conditions), confirming that the observed contraction dyssynergia is attributable to paracrine signaling dysregulation rather than cell death.

3.4. Connective tissue growth factor-mediated paracrine signaling mechanism

This section explores the paracrine signaling pathway involving CTGF in the pathological microenvironment

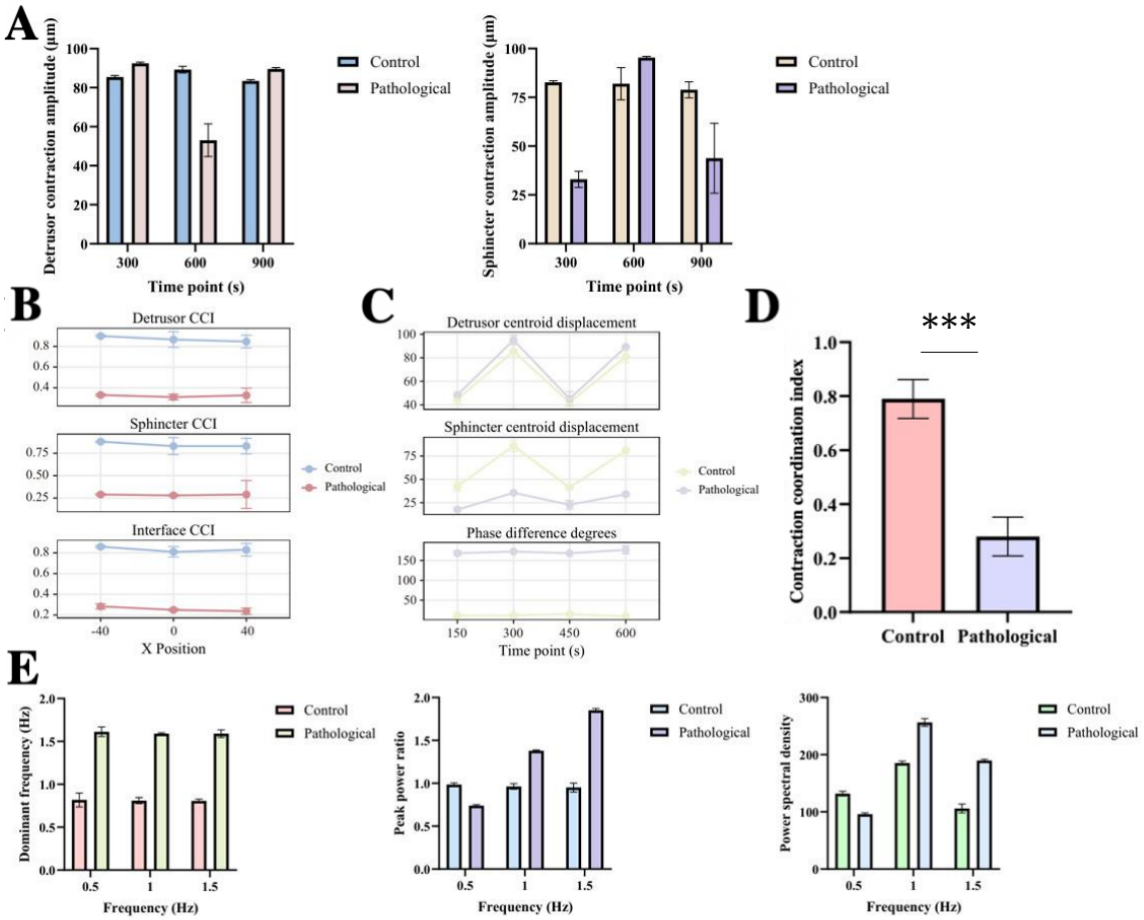

Figure 3. Phenotypic characterization of contraction dyssynergia induced by a pathological microenvironment. (A) Time-course of detrusor contraction amplitude in the bioprinted dual-tissue constructs under normal and pathological conditions. Contraction amplitude of the detrusor strips over time (0–900 s) is shown for the control and pathological groups. The control group exhibits higher contraction amplitude than the pathological group at 300, 600, and 900 s. (B) Dynamic analysis of tissue displacement by particle image velocimetry reveals uniformity score and vector fields in control and pathological conditions. (C) Quantitative comparison of centroid displacement time series showing a distinct phase difference between the detrusor and sphincter tissue in the pathological group. (D) Statistical analysis of the contraction coordination index: Control group (0.8 ± 0.04) vs. pathological group (0.26 ± 0.07), ***$p < 0.001$. (E) Power spectral density showing disturbed contraction rhythm and increased dominant frequency for the pathological group. Images in panel (A) are representative of 3 independent experiments.

and its role in contraction dyscoordination. The study aimed to elucidate which signaling molecules are essential for aberrant communication between the detrusor and sphincter in response to pathological stimulation (Figure 4). Using cytokine antibody array analysis (Figure 4A), systematic screening of the sphincter fibroblast secretome revealed that CTGF expression was significantly upregulated under pathological conditions mimicking SCI and was among the most prominently altered factors. This was quantified using ELISA, and CTGF secretion was confirmed to be increased (Figure 4B). All the results showed that the amount of CTGF secreted by sphincter fibroblasts was significantly increased (high statistical significance: *$p < 0.001$) under pathological stimulation conditions by about 8.5-fold compared to normal stimulation conditions. Quantitative PCR (qPCR) analysis (Figure 4C) further revealed a time-dependent upregulation of CTGF mRNA expression at the transcriptional level, indicating that CTGF is rapidly activated at an early stage of pathology. To directly validate CTGF function, the model was treated with recombinant CTGF (Figure 4D). The results showed that exogenous CTGF significantly reduced the CCI in a dose-dependent manner, successfully recapitulating the contraction dyscoordination phenotype. Western blot analysis (Figure 4E) demonstrated that, under pathological stimulation, the protein expression

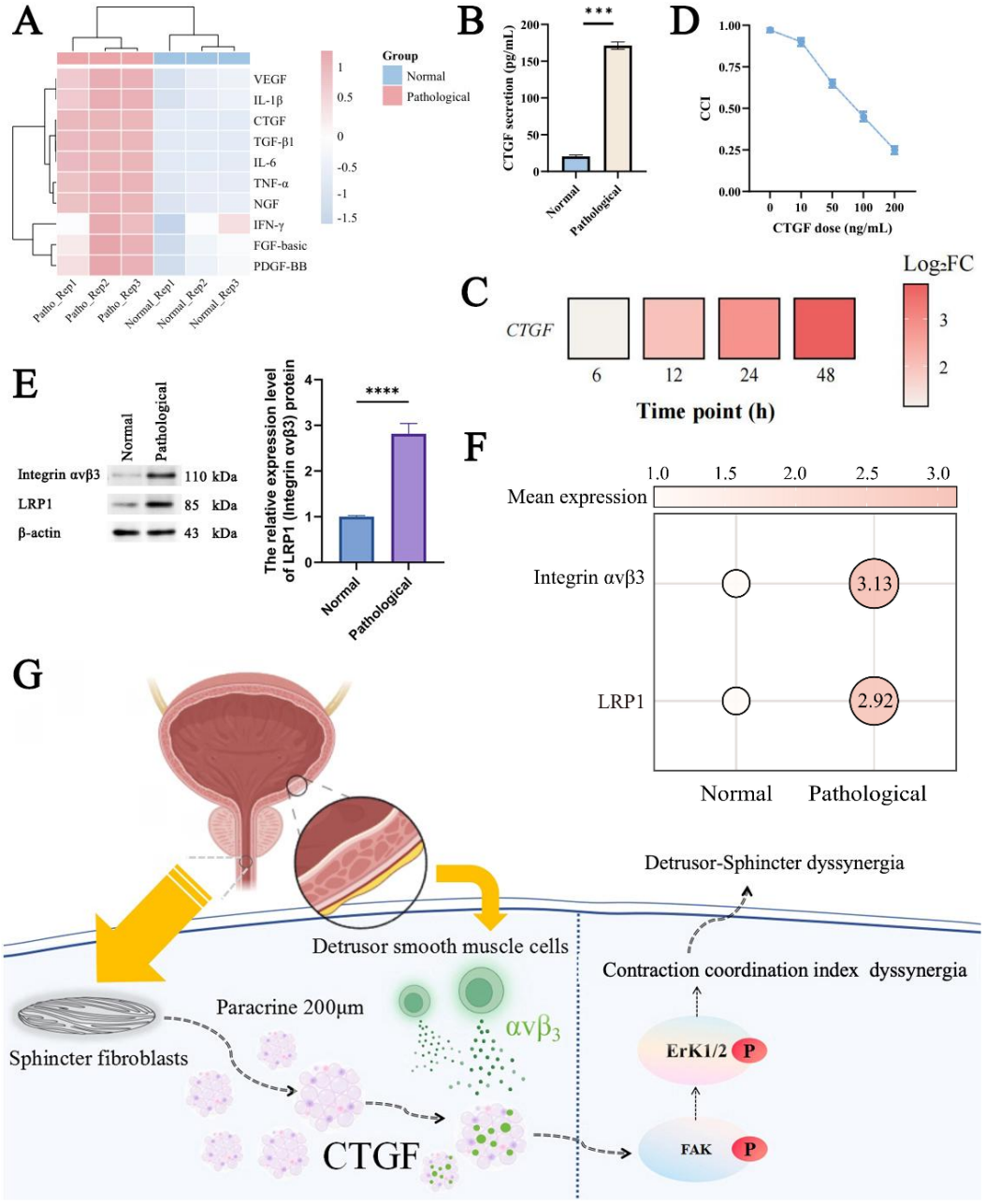

Figure 4. Mechanism of CTGF-mediated paracrine signaling in contraction dyssynergia. (A) Cytokine antibody array heatmap analysis of secretome profiles of normal and pathological sphincter fibroblasts, indicating that CTGF is a significantly increased factor. (B) Enzyme-linked immunosorbent assay showing an 8.5-fold increase (***$p < 0.001$) in the secretion of CTGF from the sphincter fibroblasts in pathological stimulation compared to normal cells. (C) Time-dependent upregulation of CTGF mRNA expression in sphincter fibroblasts under pathological conditions, as measured using quantitative polymerase chain reaction. (D) Dose-dependent reduction in CCI induced by recombinant CTGF treatment, recapitulating the pathological phenotype. (E) Western blot analysis revealed that the expression levels of the CTGF receptors integrin αvβ3 and LRP1 were both significantly upregulated in detrusor smooth muscle cells under pathological stimulation. (F) Upregulation of CTGF receptors (integrin αvβ3 and LRP1) in detrusor smooth muscle cells under pathological stimulation. (G) Schematic diagram of CTGF-mediated paracrine signaling. Under pathological stimulation, sphincter fibroblasts secrete high levels of CTGF, which diffuses across the 200 μm inter-tissue gap and binds to integrin αvβ3 on detrusor cell membranes, sequentially activating FAK and ERK1/2 phosphorylation and leading to detrusor-sphincter contraction dyscoordination (decreased CCI). Images in Panel E are representative of three independent experiments.

Notes: *$p < 0.05$; **$p < 0.01$; ***$p < 0.001$; ****$p < 0.0001$.

Abbreviations: CCI: Contraction coordination index; CTGF: Connective tissue growth factor; ERK: Extracellular signal-regulated kinase; FAK: Focal adhesion kinase; FC: Fold change; LRP1: Lipoprotein receptor-related protein 1.

levels of the CTGF receptors—integrin αvβ3 and LRP1—in detrusor smooth muscle cells were significantly higher than those in the normal group. Furthermore, quantitative analysis revealed that, in the pathological group, integrin αvβ3 expression was approximately 3.13 times that of the normal group, and LRP1 expression was approximately 2.92-fold that of the normal group (Figure 4F), suggesting that both are involved in CTGF signaling, albeit with a weaker role for LRP1 compared to integrin αvβ3, which warrants further investigation. (Figure 4G) provides a visual representation of the complete cascaded regulatory mode of CTGF-mediated paracrine signaling: at the anatomical level, sphincter fibroblasts serve as the signal source, releasing large amounts of CTGF in a paracrine manner within an inter-tissue distance of 200 μm, which diffuses to adjacent detrusor smooth muscle cells. After binding to integrin αvβ3 that is highly expressed on the detrusor cell membrane, CTGF sequentially triggers the phosphorylation and activation of FAK and ERK1/2 proteins, thereby disrupting the CCI between the detrusor and the sphincter and ultimately inducing DSD. The accompanying quantitative results also confirmed that LRP1 expression in the pathological group was significantly higher than that in the normal group, further supporting the aberrant activation of this signaling axis in the pathological microenvironment. Taken together, the data in Figure 4 allow a systematic identification and validation of CTGF as one of the important molecules secreted by the pathological microenvironment of the sphincter fibroblast, which in turn may subvert the detrusor contractile function by a paracrine effect. This offers a clear molecular target to understand the mechanism of local cellular communication that causes DSD.

3.5. The αvβ3–FAK/ERK downstream signaling pathway of connective tissue growth factor

In this section, we further dissected the downstream signaling pathway by which CTGF induces contraction dyscoordination and identified the core role of the integrin αvβ3–FAK/ERK signaling axis, focusing on how CTGF converts its extracellular signal into intracellular responses driving aberrant detrusor contraction (Figure 5). Immunofluorescence staining (Figure 5A) showed that under pathological conditions, integrin αvβ3 underwent significant clustering and altered localization on the detrusor cell membrane with markedly increased membrane intensity compared to the normal group ($p < 0.001$), suggesting its activation as a key membrane receptor for CTGF. Western blot analysis (Figure 5B) revealed the signaling kinetics: upon CTGF stimulation, phosphorylation levels of FAK (Tyr397) and ERK1/2 increased in a time-dependent manner at 0, 6, 12, and 24 h, with the ratios of phosphorylated to total FAK and ERK continuously rising within 24 h, indicating sustained pathway activation. Intervention with the specific inhibitor cilengitide (Figure 5C) completely blocked CTGF-induced FAK and ERK1/2 phosphorylation, demonstrating that integrin αvβ3 is an indispensable receptor for upstream CTGF signaling. Genetic evidence via siRNA knockdown of integrin αvβ3 (Figure 5D) not only reduced integrin expression but also reversed CTGF-induced aberrant FAK/ERK phosphorylation and, more significantly, mitigated the disruptive effect of CTGF on the CCI, with CCI values remaining near normal levels even upon CTGF stimulation. Rescue experiments using the FAK-specific inhibitor (FAK inhibitor 14) and the ERK pathway inhibitor (U0126) (Figure 5E) significantly ameliorated contraction dyscoordination induced by pathological conditions, functionally validating FAK and ERK as therapeutic targets downstream of this pathway. Figure 5F revealed that the activation folds of pFAK, pERK, and integrin β3 were all significantly increased under pathological conditions on the heatmap. Additional evidence of the overall activation of this signaling axis in DSD. These results together systematically outline the entire molecular mechanism by which CTGF acts on integrin αvβ3, which then triggers the intracellular FAK/ERK signaling pathway, which ultimately results in contractile dysfunction, and thus provide a definitive molecular target for the development of new therapeutic strategies.

3.6. Therapeutic interventions and model validation

In the final part, we focused on validating therapeutic interventions and translating the model, demonstrating the direct clinical therapeutic potential of the mechanisms identified in this study (Figure 6). First, at the *in vitro* model level, we validated the efficacy of therapeutic strategies targeting the discovered mechanisms. For the model intervention, we used mirabegron, a β3-adrenergic receptor (AR) agonist clinically approved for overactive bladder. The results indicated that the pathological group had impaired contraction coordination (CCI = 0.26), which could be significantly recovered by treatment with 10 μM mirabegron (CCI = 0.75, Figure 6A). Additional dose-response experiments (Figure 6B) indicated that the therapeutic effects of mirabegron were concentration-dependent between 1 and 20 μM, and plateaued at 10 μM, which was used as an *in vitro* reference dosage. In particular, combination therapy experiments (Figure 6C) showed that co-administration of the CTGF-neutralizing antibody with mirabegron resulted in a synergistic effect, further increasing the CCI to 0.88, significantly higher than the CCI of either therapy alone. This indicates that combined targeting of the neural receptor (β3-AR) and

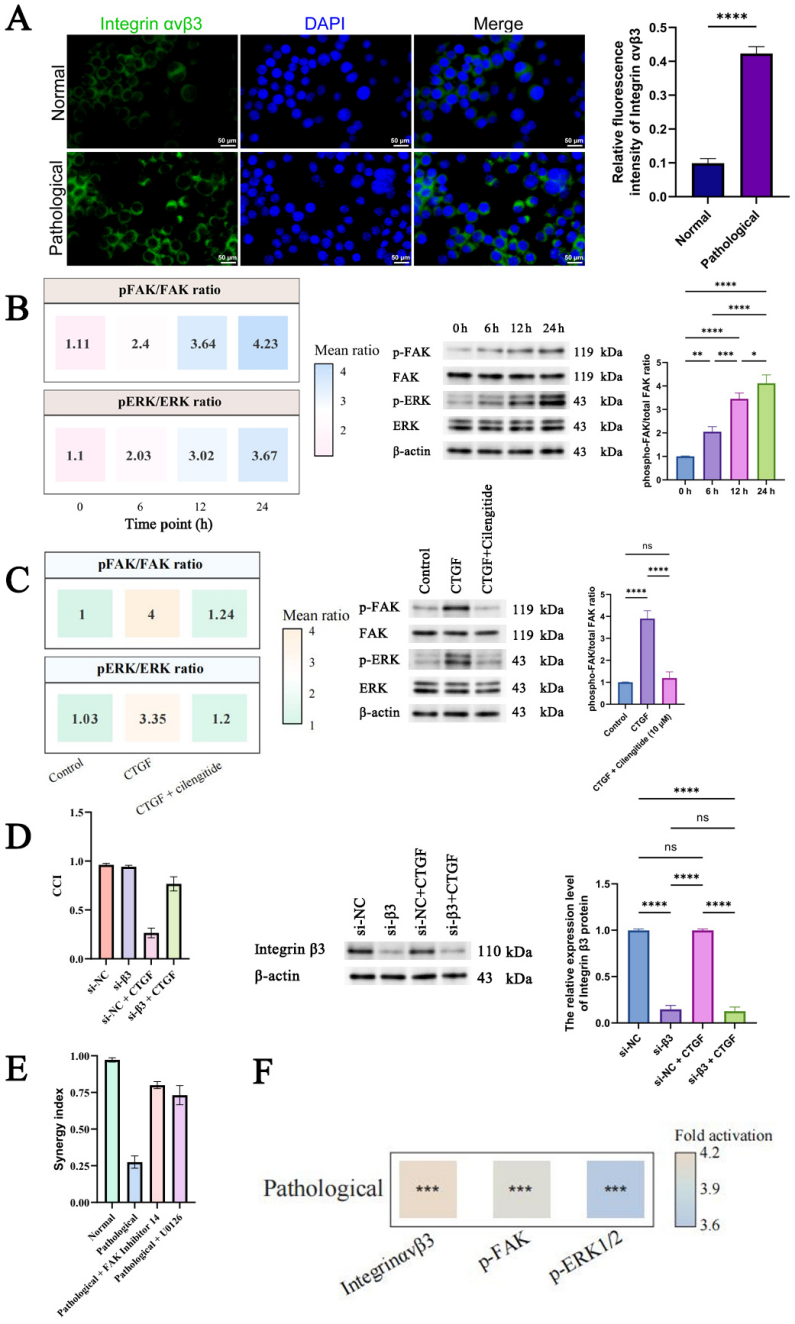

Figure 5. Dissection of the CTGF downstream signaling pathway. (A) Immunofluorescence images show enhanced membrane localization of integrin αvβ3 in detrusor cells under pathological conditions compared to normal conditions. Quantification confirmed a significant increase in membrane signal intensity ($p < 0.001$). Scale bar: 50 μm; magnification: 40×. (B) Western blot analysis revealed time-dependent increases in FAK (Tyr397) and ERK1/2 phosphorylation at 0, 6, 12, and 24 h upon CTGF stimulation. The p-FAK/FAK and p-ERK/ERK ratios rose continuously within 24 h. (C) The integrin αvβ3 inhibitor cilengitide suppressed CTGF-induced FAK and ERK1/2 phosphorylation, returning levels to near baseline. (D) CCI for four groups (si-NC, si-β3, si-NC + CTGF, si-β3 + CTGF). siRNA knockdown of integrin β3 reduced integrin αvβ3 expression and reversed CTGF-induced aberrant FAK/ERK phosphorylation. (E) Statistical analysis of the contraction coordination index for four groups: pathological stimulation significantly decreased the index, while treatment with FAK inhibitor 14 or the ERK pathway inhibitor (U0126) significantly rescued contraction coordination, functionally validating the potential of FAK and ERK as therapeutic targets downstream of this pathway. (F) Heatmap showing that activation folds (relative to normal) of p-FAK, p-ERK, and integrin β3 were all significantly elevated under pathological conditions. Images in Panels A–D are representative of three independent experiments. Notes: Data are presented as mean ± standard deviation ($n = 3$); $^{*}p < 0.05$, $^{**}p < 0.01$, $^{***}p < 0.001$, $^{****}p < 0.0001$; ns: not significant ($p \geq 0.05$). Abbreviations: CCI: Contraction coordination index; CTGF: Connective tissue growth factor; DAPI: 4',6-diamidino-2-phenylindole; ERK: Extracellular signal-regulated kinase; FAK: Focal adhesion kinase; si-NC: Normal control siRNA.

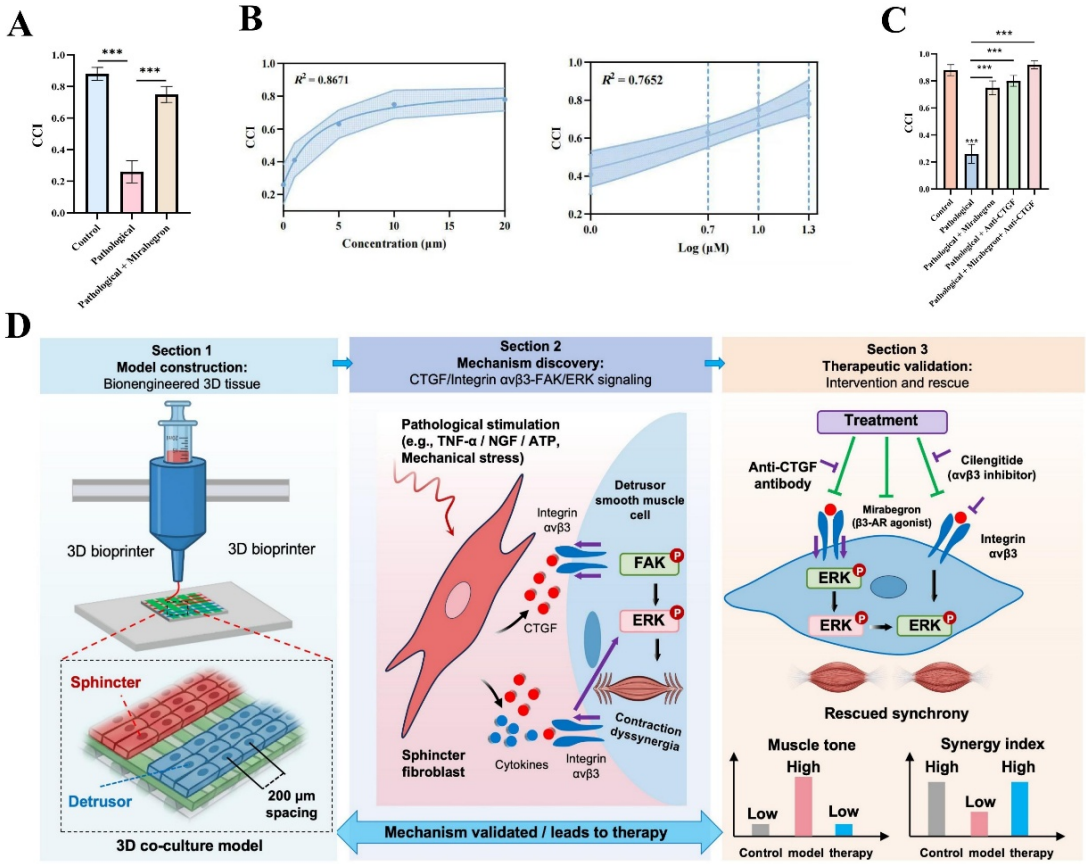

Figure 6. Therapeutic interventions and model validation. (A) Mirabegron treatment (10 μM) significantly improved the contraction coordination index (CCI) from 0.26 (pathological group) to 0.75 (***$p < 0.001$). (B) Mirabegron dose-response curve for restoration of CCI. A concentration-dependent effect was observed from 1 to 10 μM, after which the response plateaued. (C) Mirabegron (10 μM), when combined with a CTGF-neutralizing antibody, significantly enhanced CCI compared to the monotherapies (***$p < 0.001$). (D) A schematic summary of the entire research pipeline from the establishment of the model, dissection of the mechanism, and therapeutic validation, which represents the full process from basic research to translational applications.

of the local paracrine signaling (CTGF) could be a more effective therapeutic approach. The entire research journey from model establishment to mechanism dissection and therapeutic validation was summarized in the schematic (Figure 6D), which represents a closed loop from basic discovery to translation.

4. Discussion

In this study, a spatially defined 3D bioprinting approach was used to create an *in vitro* paracrine communication model of the detrusor and urethral sphincter. It reveals that the pathological microenvironment following SCI triggers CTGF secretion from sphincter fibroblasts, activates the integrin αvβ3–FAK/ERK pathway in the detrusor cells, and ultimately causes DSD. To the best of our knowledge, this study is the first to allow visualization and quantitative analysis of the contractile function of DSD, as well as demonstrating a paracrine mechanism that operates in the absence of direct neural input of coordination disruption involving the CTGF/integrin αvβ3–FAK/ERK signaling axis and establishes the therapeutic potential of combination therapy with mirabegron and a CTGF-neutralizing antibody.

Detrusor-sphincter dyssynergia is commonly caused by an imbalance in central neural control circuitry after SCI. However, this study demonstrates that, even in the complete absence of neural innervation and direct cell–cell contact, contraction dyscoordination between the detrusor and sphincter can be recapitulated *in vitro* solely through paracrine signaling induced by the pathological microenvironment. This suggests that local intercellular signaling disturbances may represent a pathogenic factor independent of neural injury. By setting a precise inter-tissue distance of 200 μm, the model achieves a "separated-but-communicating" coculture, preserves a 3D

extracellular matrix environment and dynamic contractile function, and enables real-time quantification via the CCI. Compared to traditional methods, this approach avoids interference from direct cell–cell contact;[11] compared to animal models, it allows the isolated study of paracrine signaling. Most existing bioprinting studies have focused on single tissues;[20] this study upgrades bioprinting into a mechanistic dissection platform to directly test paracrine-dependent contraction coordination.

Connective tissue growth factor is a key factor promoting fibrosis, cell proliferation, and extracellular matrix deposition.[21] In the bladder, it has been associated with fibrosis following bladder outlet obstruction.[21,27] The present study identifies CTGF as a paracrine signaling molecule that directly disrupts phase synchrony of contractions between the detrusor and the sphincter. Upon pathological stimulation, CTGF was upregulated approximately 8.5-fold, and CTGF decreased the CCI in a dose-dependent manner (from 0.8 to 0.26). Unlike the role of CTGF in various tissue fibrosis through binding to integrin αvβ3,[22] this study extends its function to the regulation of smooth muscle contraction coordination, suggesting that CTGF may serve as a bridge molecule linking "tissue remodeling" and "dysfunction." This study systematically dissects the downstream signaling pathway by which CTGF induces aberrant detrusor contraction. CTGF binds to integrin αvβ3 (rather than its canonical receptor LRP1) on the detrusor cell membrane, activates FAK and ERK1/2 phosphorylation, and ultimately leads to contraction dyscoordination. Although CTGF can bind multiple integrins (e.g., αvβ3, α6β1)22, our study identified the αvβ3–FAK/ERK axis as the dominant pathway regulating smooth muscle contractile function. The FAK/ERK pathway has previously been associated mainly with cell migration, proliferation, or fibrosis;[23] the present study directly links it to the phase synchrony of contraction rhythms. Treatment with cilengitide, a FAK inhibitor 14, or U0126 completely blocked the CTGF effect, validating the necessity of this pathway from two independent lines of evidence.

The mechanisms by which the SCI-mimetic inflammatory cocktail (TNF-α/NGF/ATP) specifically upregulates CTGF in sphincter fibroblasts warrant further consideration. Although upstream signaling was not directly measured in the present study, several well-characterized pathways may link inflammatory stimulation to CTGF transcription. TNF-α is a potent activator of the nuclear factor (NF)-κB pathway; upon receptor activation, inhibitor of nuclear factor kappa B (IκB) is phosphorylated by IκB kinase, leading to IκB degradation, NF-κB nuclear translocation, and binding to κB sites within the CTGF promoter, thereby driving CTGF transcription. In parallel, NGF signaling via the tropomyosin receptor kinase A receptor can activate the mitogen-activated protein kinase (MAPK) cascade, which converges on activator protein-1 and other transcription factors that regulate CTGF expression. Furthermore, transforming growth factor (TGF)-β/Smad signaling, a master regulator of CTGF, may be indirectly activated by TNF-α-induced latent TGF-β release from the extracellular matrix or via crosstalk between NF-κB and Smad transcriptional complexes.[28,29] ATP released under pathological conditions may further amplify CTGF expression through purinergic P2X/P2Y receptor-mediated calcium and MAPK signaling. Future studies employing pharmacological inhibition of NF-κB (e.g., BAY 11-7082), TGF-β receptor blockade (e.g., SB-431542), and chromatin immunoprecipitation for NF-κB and Smad occupancy at the CTGF promoter are warranted to definitively establish the upstream regulatory network linking the SCI-mimetic microenvironment to CTGF secretion in sphincter fibroblasts.[30]

A mechanistic cascade model is proposed in our study in which the pathological microenvironment, characterized by elevated TNF-α, NGF, and ATP signaling, induces excessive CTGF secretion from sphincter fibroblasts. The secreted CTGF subsequently diffuses across the 200-μm interface gap and interacts with integrin αvβ3 expressed on the detrusor surface, resulting in activation of downstream FAK and ERK1/2 signaling pathways. This aberrant signaling may disrupt intracellular contractile regulation, potentially through alterations in calcium homeostasis and/or myosin light chain phosphorylation, leading to impaired smooth muscle coordination. Consequently, the temporal relationship between detrusor and sphincter contractions becomes desynchronized, resulting in reduced CCI and the emergence of a DSD phenotype.[31]

Mirabegron is a β3-AR agonist clinically used to treat an overactive bladder.[24] The present study found that mirabegron restored the CCI under pathological conditions in a concentration-dependent manner (from 0.26 to 0.75 at 10 μM), an effect comparable to that of a CTGF-neutralizing antibody. Mechanistically, β3-AR activation increases intracellular cyclic adenosine monophosphate (cAMP), which in turn regulates smooth muscle relaxation.[32] The advantage of combination therapy lies in simultaneously targeting neural regulation (β3-AR) and local paracrine signaling (CTGF), which may be particularly beneficial for patients with potential downregulation of β3-AR expression after neural injury, where the CTGF pathway can serve as a synergistic target. Compared to existing treatments (α-blockers, anticholinergic drugs, and botulinum toxin), targeting the

CTGF/integrin αvβ3 pathway has not yet been attempted in DSD,[24] and the present study provides a theoretical basis for developing novel biologics or small-molecule inhibitors.

It should be noted that β3-AR expression was not directly measured in the printed detrusor cells or dual-tissue constructs in our study. Therefore, the possibility that the observed restoration of CCI by mirabegron may involve off-target effects cannot be definitively excluded. However, substantial evidence from the literature supports the presence of functional β3-AR in bladder detrusor smooth muscle. At the mRNA level, β3-AR is the predominant β-AR subtype expressed in the human detrusor, accounting for approximately 97% of total β-AR mRNA.[33] At the protein level, β3-AR expression has been confirmed in human detrusor smooth muscle via immunohistochemistry and western blotting. In cultured human and rat detrusor smooth muscle cells, β3-AR expression is maintained and functional, as evidenced by mirabegron-induced cAMP accumulation and cell relaxation. Furthermore, mirabegron is clinically approved for overactive bladder based on its selective β3-AR agonism in the detrusor, providing indirect but strong evidence for β3-AR expression in the bladder wall.[34] Nevertheless, future studies should verify β3-AR expression in the printed detrusor constructs using qPCR and immunofluorescence staining, and confirm target specificity using β3-AR-selective antagonists (e.g., L-748, 337) or siRNA-mediated β3-AR knockdown in the bioprinted model. Importantly, as the present study did not directly measure β3-AR expression in the printed detrusor cells, future studies employing selective β3-AR antagonists (e.g., L-748, 337) or β3-AR knockdown (siRNA) in the bioprinted model are warranted to definitively confirm target specificity.

Despite the insights provided by this study, several limitations should be acknowledged. Fibroblasts were used as urethral sphincter components rather than the physiologically active striated muscle cells. This allowed evaluation of the paracrine signal output, but it did not fully mimic the active contractile function of the sphincter. This model does not incorporate neural and vascular networks, unlike the *in vivo* microenvironment.[35] The direct effect of CTGF on the oscillation of calcium and/or myosin light chain phosphorylation in the detrusor cells through the FAK/ERK pathway is not directly determined. Translation evidence in the clinical setting remains scarce, and the feasibility of CTGF as a biomarker should be validated on a large scale. Additionally, the molecular mechanism by which ERK1/2 phosphorylation leads to detrusor smooth muscle cell asynchronous contraction remains unclear, although this study demonstrates that CTGF activates the FAK/ERK pathway. Several plausible hypotheses merit consideration: (i) ERK may directly or indirectly phosphorylate myosin light chain kinase and/or the regulatory myosin light chain, altering the force-generating capacity and rhythmicity of individual smooth muscle cells;[36] (ii) ERK activation may modulate intracellular calcium homeostasis by regulating the activity of L-type voltage-gated calcium channels (Cav1.2), store-operated calcium entry, or sarcoplasmic reticulum Ca^{2+}-ATPase, thereby desynchronizing the calcium oscillations that drive rhythmic contraction;[37] (iii) ERK signaling may downregulate the expression or phosphorylation of gap junction proteins, particularly Connexin 43 (Cx43), which is the predominant gap junction subunit in detrusor smooth muscle and is essential for electrical coupling and synchronous contraction of the bladder wall. Of these, the gap junction hypothesis is particularly attractive, as Cx43 downregulation has been documented in bladder dysfunction models and ERK-dependent Cx43 phosphorylation at serine residues (e.g., Ser279/282) is known to reduce gap junction communication.[38] These hypotheses should be tested in future studies using calcium imaging, patch-clamp electrophysiology, and Cx43-specific interventions (e.g., Gap27 peptide, Cx43 overexpression) in the bioprinted model.[39,40]

Future studies should focus on further advancing this platform toward a more physiologically representative and clinically relevant model of DSD. A three-component system integrating neurons, smooth muscle cells, and fibroblasts could be developed by incorporating motor neurons and sphincter striated muscle cells to investigate the complex interplay between neural regulation and paracrine signaling.[26] In addition, vascularization and immune cell coculture could be introduced to better simulate the effects of inflammatory infiltration on the paracrine network following SCI.[41] Functional studies incorporating calcium imaging or patch-clamp electrophysiology would enable real-time assessment of electrophysiological alterations in detrusor cells in response to CTGF stimulation. Furthermore, the high-throughput capability of this platform could facilitate screening of small-molecule inhibitors targeting the CTGF/αvβ3 signaling axis and optimization of their combination with mirabegron for potential therapeutic applications. Finally, multicenter clinical studies assessing CTGF levels in urine or tissue samples from DSD patients across different disease stages will be essential for validating CTGF as a biomarker and establishing a non-invasive diagnostic strategy.

5. Conclusion

In this study, we developed a spatially defined bioprinting strategy and established the first *in vitro* model for

quantitative assessment of detrusor-sphincter contraction coordination. Using this platform, we revealed a novel paracrine-based mechanism of DSD: after SCI, the local pathological microenvironment induces aberrant CTGF secretion from sphincter fibroblasts,[42] which activates the integrin αvβ3–FAK/ERK pathway and leads to detrusor dysregulation. We also validated the therapeutic potential of mirabegron combined with a CTGF-neutralizing antibody. These findings offer new insights into DSD pathophysiology and provide a theoretical basis for therapies targeting inter-tissue communication.

Acknowledgments

None.

Funding

This work was supported by the General Program of Shanxi Provincial Natural Science Foundation (No. 202503021211298) and the National Natural Science Foundation of China (82470809).

Conflict of interest

The authors declare there are no competing interests.

Author contributions

Conceptualization: Weilun Zhang, Lei Pang
Formal analysis: Weilun Zhang, Yuxin Zhang, Xueling Yan, Junya Shi
Investigation: Weilun Zhang, Yuxin Zhang, Yuexian Liu, Yutong Li, Yipeng Zhao, Zhen Zhang, Wenbo Zhai, Yi Rong, Jingtang Hu
Methodology: Weilun Zhang, Yuxin Zhang, Chengzhi Zhang, Haowei Song, Xiaodong Wen
Resources: Weibing Shuang, Lei Pang
Writing–original draft: Weilun Zhang, Chengzhi Zhang, Lei Pang
Writing–review & editing: Lei Pang

Ethics approval and consent to participate

This study involved isolation of primary fibroblasts from rat urethral sphincter tissue and the use of commercial rat primary bladder smooth muscle cells. All animal procedures were approved by the Animal Ethics Committee of Shanxi Medical University (approval number: 2026(675)). The study complied with the Guide for the Care and Use of Laboratory Animals.

Consent for publication

Not applicable.

Availability of data

The data used in this study (including raw time-lapse contraction images, western blot bands, qPCR data, etc.) are available from the corresponding authors upon reasonable request.

References

1. Pereira JA, Debugne T. Evaluation methods of detrusor sphincter dyssynergia in spinal cord injury patients: a literature review. *Uro*. 2022;2(2):122-133.

   doi: 10.3390/uro2020015

2. Furrer MA, Kessler TM, Panicker JN. Detrusor sphincter dyssynergia. *Urol Clin North Am*. 2024;51(2):221-232.

   doi: 10.1016/j.ucl.2024.01.001

3. Feloney MP, Leslie SW. Bladder sphincter dyssynergia. StatPearls [Internet]. Treasure Island (FL): StatPearls Publishing. Updated November 12, 2023. Accessed January 7, 2026. https://www.ncbi.nlm.nih.gov/books/NBK562166/

4. Ruan J, Ou T, Cui X, Yan H, Cui B, Shang Z. Decoding the ceRNA regulatory landscape: a comprehensive transcriptomic analysis of ncRNA-driven bladder fibrosis following spinal cord injury. *Transl Androl Urol*. 2025;14(10):3003-3022.

   doi: 10.21037/tau-2025-376

5. Wyndaele M, Charrua A, Hervé F, *et al.* Beyond the urothelium: interplay between autonomic nervous system and bladder inflammation in urinary tract infection, bladder pain syndrome with interstitial cystitis and neurogenic lower urinary tract dysfunction in spinal cord injury—ICI-RS 2023. *Neurourol Urodyn*. 2024;43(6):1283-1292.

   doi: 10.1002/nau.25310

6. Liang C-C, Shaw S-WS, Ko Y-S, Huang Y-H, Lee T-H, *et al.* Effect of amniotic fluid stem cell transplantation on the recovery of bladder dysfunction in spinal cord-injured rats. *Sci Rep*. 2020;10(1):10030.

   doi: 10.1038/s41598-020-67163-7

7. Huang MS, Christakopoulos F, Roth JG, Heilshorn SC. Organoid bioprinting: from cells to functional tissues. *Nat Rev Bioeng*. 2024;3(2):126-142.

   doi: 10.1038/s44222-024-00268-0

8. Cao S, Ma H, Wu C. Biomaterials-modulated multicellular crosstalk in 3D bioprinted constructs. *Adv Interv Mater*. 2026;1(1):100008.

   doi: 10.1016/j.advim.2025.100008

9. Du L, Lu Y, Yang H. Three-dimensional (3D) bioprinted co-culture models: a new paradigm for reproducing the tumor microenvironment and precision therapy. *Hepatobiliary Surg Nutr*. 2025;14(3):482-485.

   doi: 10.21037/hbsn-2025-297

10. Hu M, Dong L, Gao Y, *et al.* 3D sheng wu da yin yan jiu zhan wang ji xiang lin chuang qian dong wu mo xing de kua xue

ke ying yong. [Prospects for 3D bioprinting research and transdisciplinary application to preclinical animal models]. *Lab Anim Comp Med*. 2025;45(3):318-330. [In Chinese]

doi: 10.12300/j.issn.1674-5817.2024.193

11. Jeon S, Heo J-H, Kim MK, Jeong W, Kang H-W. High-precision 3D bio-dot printing to improve paracrine interaction between multiple types of cell spheroids. *Adv Funct Mater*. 2021;30(52):2005324.

doi: 10.1002/adfm.202005324

12. Yong U, Park J, Jang J. Bioprinted excitable tissues with multistimulation systems for promoting function and maturation. *Adv NanoBiomed Res*. 2026;6(3).

doi: 10.1002/anbr.202500107

13. Rea M, Di Lisa L, Pagnotta G, *et al.* Establishing a bioink assessment protocol: GelMA and collagen in the bioprinting of a potential in vitro intestinal model. *ACS Biomater Sci Eng*. 2025;11(4):2456-2467.

doi: 10.1021/acsbiomaterials.5c00034

14. Jeong W, Han J, Choi J, Kang H-W. Embedded bioprinting of breast cancer-adipose composite tissue model for patient-specific paracrine interaction analysis. *Adv Healthc Mater*. 2025;e2401887.

doi: 10.1002/adhm.202401887

15. Ben-Gida H, Gurka R, Liberzon A. OpenPIV-MATLAB—An open-source software for particle image velocimetry; test case: birds' aerodynamics. *SoftwareX*. 2020;12:100585.

doi: 10.1016/j.softx.2020.100585

16. Dickman CTD, Russo V, Thain K, *et al.* Functional characterization of 3D contractile smooth muscle tissues generated using a unique microfluidic 3D bioprinting technology. *FASEB J*. 2020;34(1):1652-1664.

doi: 10.1096/fj.201901063RR

17. Lee HL, Kim B, Yun J, *et al.* PIV-MyoMonitor: an accessible particle image velocimetry-based software tool for advanced contractility assessment of cardiac organoids. *Front Bioeng Biotechnol*. 2024;12:1367141.

doi: 10.3389/fbioe.2024.1367141

18. Szabó A, Pasquariello R, Costa PF, *et al.* Light-based 3D printing of gelatin-based biomaterial inks to create a physiologically relevant in vitro fish intestinal model. *Macromol Biosci*. 2023;23(10):e2300016.

doi: 10.1002/mabi.202300016

19. Guo DY, Chen ZH, Fu YF, *et al.* Cilengitide inhibits osteoclast adhesion through blocking the αvβ3-mediated FAK/Src signaling pathway. *Heliyon*. 2023;9(7):e17841.

doi: 10.1016/j.heliyon.2023.e17841

20. Budharaju H, Singh RK, Kim HW. Bioprinting for drug screening: A path toward reducing animal testing or redefining preclinical research? *Bioact Mater*. 2025;51:993-1017.

doi: 10.1016/j.bioactmat.2025.07.006

21. Metcalfe PD, Wang J, Jiao H, *et al.* Bladder outlet obstruction: progression from inflammation to fibrosis. *BJU Int*. 2010 Dec;106(11):1686-94.

doi: 10.1111/j.1464-410X.2010.09445.x

22. Lee SY. Endothelial cell-derived connective tissue growth factor stimulates fibroblast differentiation into myofibroblasts through integrin αVβ3. *Exp Ther Med*. 2022 Nov 24;25(1):30.

doi: 10.3892/etm.2022.11730

23. Tan TW, Lai CH, Huang CY, *et al.* CTGF enhances migration and MMP-13 up-regulation via αvβ3 integrin, FAK, ERK, and NF-κB-dependent pathway in human chondrosarcoma cells. *J Cell Biochem*. 2009;107(2):345-356.

doi: 10.1002/jcb.22132

24. Tousignant A, Blais M-A, Tu L-M, Morin M, Ismail S. A scoping review of the oral treatment options for the management of detrusor sphincter dyssynergia. *Neurourol Urodyn*. 2025;44(4):743-753.

doi: 10.1002/nau.25642

25. Wang N, Zheng X, Qian J, *et al.* Renal sympathetic denervation alleviates myocardial fibrosis following isoproterenol-induced heart failure. *Mol Med Rep*. 2017;16(4):5091-5098.

doi: 10.3892/mmr.2017.7255

26. Yilmaz EG, Haciosmanoğlu N, Inci F, Ashammakhi N. Modeling the synapse and neuromuscular junction using organ-on-a-chip technology. In: *Handbook of Neural Engineering*. Amsterdam, Netherlands: Elsevier; 2025:625-643.

doi: 10.1016/B978-0-323-95730-4.00008-1

27. Altuntas CZ, Daneshgari F, Izgi K, *et al.* Connective tissue and its growth factor CTGF distinguish the morphometric and molecular remodeling of the bladder in a model of neurogenic bladder. *Am J Physiol Renal Physiol*. 2012 Nov 1;303(9):F1363-F1369.

doi: 10.1152/ajprenal.00273.2012

28. Yue K, Trujillo-de Santiago G, Alvarez MM, Tamayol A, Annabi N, Khademhosseini A. Synthesis, properties, and biomedical applications of gelatin methacryloyl (GelMA) hydrogels. *Biomaterials*. 2015;73:254-271.

doi: 10.1016/j.biomaterials.2015.08.045

29. Leask A, Abraham DJ. All in the CCN family: essential matricellular signaling modulators emerge from the bunker. *J Cell Sci*. 2006;119(23):4803-4810.

doi: 10.1242/jcs.03270

30. Mori T, Kawara S, Shinozaki M, *et al.* Role and interaction of connective tissue growth factor with transforming growth

factor-β in persistent fibrosis: a mouse fibrosis model. *J Cell Physiol*. 1999;181(1):153-159.

doi: 10.1002/(SICI)1097-4652(199910)181:1<153::AID-JCP16>3.0.CO;2-K

31. Kim HR, Appel S, Vetterkind S, Gangopadhyay SS, Morgan KG. Smooth muscle signalling pathways in health and disease. *J Cell Mol Med*. 2008;12(6A):2165-2180.

doi: 10.1111/j.1582-4934.2008.00552.x

32. Yamaguchi O. β3-adrenoceptors in human detrusor muscle. *Urology*. 2002;59(5 Suppl 1):25-29.

doi: 10.1016/S0090-4295(01)01635-1

33. Lee J, Lee E, Huh SJ, *et al.* Composite spheroid-laden bilayer hydrogel for engineering three-dimensional osteochondral tissue. *Tissue Eng Part A*. 2024;30(5-6):225-243.

doi: 10.1089/ten.TEA.2023.0299

34. Berridge MJ. Smooth muscle cell calcium activation mechanisms. *J Physiol*. 2008;586(21):5047-5061.

doi: 10.1113/jphysiol.2008.160440

35. Rayego-Mateos S, Campillo S, Rodrigues-Diez RR, *et al.* Interplay between extracellular matrix components and cellular and molecular mechanisms in kidney fibrosis. *Clin Sci (Lond)*. 2021;135(16):1999-2029.

doi: 10.1042/CS20201016

36. Martin-Aragon Baudel M, Espinosa-Tanguma R, Nieves-Cintron M, Navedo MF. Purinergic signaling during hyperglycemia in vascular smooth muscle cells. *Front Endocrinol (Lausanne)*. 2020;11:329.

doi: 10.3389/fendo.2020.00329

37. Nakamura A, Xie C, Zhang Y, *et al.* Role of non-kinase activity of myosin light-chain kinase in regulating smooth muscle contraction, a review dedicated to Dr. Setsuro Ebashi. *Biochem Biophys Res Commun*. 2008;369(1):135-143.

doi: 10.1016/j.bbrc.2007.11.096

38. Neuhaus J, Weimann A, Stolzenburg J-U, Wolburg H, Horn L-C, Dorschner W. Smooth muscle cells from human urinary bladder express connexin 43 in vivo and in vitro. *World J Urol*. 2002;20(4):250-254.

doi: 10.1007/s00345-002-0289-9

39. D'hondt C, Iyyathurai J, Vinken M, *et al.* Regulation of connexin- and pannexin-based channels by post-translational modifications. *Biol Cell*. 2013;105(9):373-398.

doi: 10.1111/boc.201200096

40. Nomiya M, Yamaguchi O. A quantitative analysis of mRNA expression of alpha 1 and beta-adrenoceptor subtypes and their functional roles in human normal and obstructed bladders. *J Urol*. 2003;170(2 Pt 1):649-653.

doi: 10.1097/01.ju.0000067621.62736.7c

41. Zhang J, Ren F, Bu F, Yao Y, Li M. 3D bioprinting-driven strategies for tissue regeneration and controlled immune modulation. *Int J Bioprint*. 2026;12(1):173-198.

doi: 10.36922/IJB025460474

42. Davies AL, Hayes KC, Dekaban GA. Clinical correlates of elevated serum concentrations of cytokines and autoantibodies in patients with spinal cord injury. *Arch Phys Med Rehabil*. 2007;88(11):1384-1393.

doi: 10.1016/j.apmr.2007.08.004